Experimental Realization of Thermal Reservoirs with Tunable Temperature in a Trapped-Ion Spin-Boson Simulator

Visal So,[1,*] Mingjian Zhu,[1] Midhuna Duraisamy Suganthi,[1,2] Abhishek Menon,[1] George Tomaras,[1,2] Roman Zhuravel,[1] Han Pu,[1] and Guido Pagano[1,†]

[1]Department of Physics and Astronomy and Smalley-Curl Institute, Rice University, Houston, Texas 77005, USA
[2]Applied Physics Graduate Program, Smalley-Curl Institute, Rice University, Houston, Texas 77005, USA

(Received 19 November 2025; revised 6 February 2026; accepted 10 July 2026; published 30 July 2026)

We propose and demonstrate an experimental scheme to engineer thermal baths with independently tunable temperatures and dissipation rates for the motional modes of a trapped-ion system. This approach enables robust thermal-state preparation and quantum simulations of open-system dynamics in bosonic and spin-boson models at well-controlled finite temperatures. We benchmark our protocol by experimentally realizing out-of-equilibrium dynamics of a charge-transfer model at different temperatures. We observe that, when the process occurs at a higher temperature, the transfer rate spectrum broadens, with reduced rates at small donor-acceptor energy gaps and enhanced rates at large gaps. We then employ our scheme to study local-temperature effects in a two-mode vibrationally assisted exciton transfer system, where we observe thermally activated interference pathways for excitation transfer.

DOI: 10.1103/mf8d-91ws

Introduction—The competition between Coulomb interactions and trapping potentials in trapped-ion crystals gives rise to effective harmonic oscillator modes that describe the collective ion motion. Although these modes can serve as native degrees of freedom for quantum applications, complementing the internal electronic states of the ions, they have more commonly been used as mediators for qubit-qubit interactions [1]. Consequently, experimental efforts have traditionally focused on keeping these bosonic degrees of freedom near the ground state by optimizing cooling techniques and mitigating heating mechanisms to minimize temperature-related errors in quantum computing and simulation [2–4]. However, the use of trapped-ion bosonic modes as information carriers and active degrees of freedom in purely bosonic and spin-boson models has recently attracted growing interest [5,6]. Nonclassical motional states in trapped-ion systems have been used to encode continuous-variable logical states [7–9], which are promising tools for efficient error correction [10–12]. Moreover, by engineering phonon-phonon couplings mediated by the ions' spin degrees of freedom or employing the anharmonicity of the Coulomb potential, the harmonic oscillator quanta themselves can act as computational units, enabling boson sampling and simulations of bosonic Hamiltonians [13–18].

In addition, treating spin and bosonic degrees of freedom on equal footing allows us to efficiently simulate spin-boson systems through digital [19,20] or analog protocols [21–26]. In analog simulations, native interactions between the ions' degrees of freedom and controlled electromagnetic fields engineer target spin-boson Hamiltonians, including linear vibronic coupling (LVC) models for studying key chemical processes, such as charge transfer and dissociation [27–30]. Combined with reservoir-engineering techniques, this approach extends naturally to open-system dynamics, where environmental effects are non-negligible [6,31,32]. Therefore, trapped-ion thermal-reservoir engineering can support quantum applications by enabling thermal-state preparation and studies of open-system dynamics. Since many chemical-reaction models assume global thermal equilibrium between the system and its surroundings [33–35], the ability to establish a finite-temperature reservoir paves the way to experimentally study these processes under realistic thermodynamic conditions. Moreover, such reservoirs enable experimental studies of thermal entanglement [36], temperature-dependent decoherence [37], and heat flow across temperature gradients [38].

Existing reservoir-engineering techniques in trapped-ion systems provide a well-established toolkit for tailoring motional states. Many approaches rely on cooling processes [39–43], which pump the system into the vacuum state [44] or squeezed and entangled states [45–48]. Effectively thermal reservoirs can be realized through noise injection [3,49] and stochastic processes [50], which commonly produce high- or infinite-temperature steady

*Contact author: vs39@rice.edu
†Contact author: pagano@rice.edu

Published by the American Physical Society under the terms of the Creative Commons Attribution 4.0 International license. Further distribution of this work must maintain attribution to the author(s) and the published article's title, journal citation, and DOI.

states. On the other hand, controlled competition between heating and cooling processes has been employed to study phase transitions in the motional state [51] and to realize quantum Van der Pol oscillators using combinations of linear and nonlinear dissipation channels [52].

In this Letter, we focus on a distinct method that combines controlled heating and cooling of trapped ions' motional modes to engineer thermal baths with independently tunable temperature and dissipation rate. Experimentally, we induce motional excitation by broadcasting an electric-field signal with stochastic phases and remove phonon energy via laser cooling. We test this scheme on a dual-species ion chain to probe temperature effects in a charge-transfer model, observing a broadening of the transfer rate spectrum with respect to the donor-acceptor energy gap at higher temperatures. We also explore the role of local temperature in a two-mode system, where vibrationally assisted transfer exhibits thermal activation of coherent transfer pathways. Our Letter provides a key-enabling tool for studying open quantum systems under the influence of thermal environments, with direct relevance to real chemical systems (e.g., proton-coupled electron transfer in catalysis [53]), biological systems (e.g., exciton transfer in photosynthetic complexes [54]), and physical systems (e.g., phonon-induced decoherence in solid-state qubits [55]) as well as for dissipative thermal-state preparation, useful for applications in quantum information science.

Theory—Throughout this Letter, we adopt the convention of setting $\hbar = 1$. By simultaneously implementing cooling and heating processes on any chosen motional mode of a trapped-ion system at rates γ_c and γ_h, respectively, the dynamics of the system is given by

$$\frac{\partial\rho}{\partial t} = -i[H,\rho] + \gamma_c(n_{\rm ss}+1)\mathcal{D}_a[\rho] + \gamma_c n_{\rm ss}\mathcal{D}_{a^\dagger}[\rho],$$
$$\mathcal{D}_c[\rho] = c\rho c^\dagger - \frac{1}{2}\{c^\dagger c,\rho\}, \tag{1}$$

where H is the total Hamiltonian of the system, $n_{\rm ss} = \gamma_h/\gamma_c$, and a and $a^\dagger$ represent the annihilation and creation operators, respectively. Considering only the dissipation terms, the steady state of the motional mode is a thermal state characterized by $n_{\rm ss} \equiv \bar{n}$ [56] (see Supplemental Material [57] for the derivation). Therefore, the dissipation rate can be controlled by γ_c, while the bath temperature can be set independently by tuning γ_h. To benchmark the effect of the thermal bath, it is convenient to track the time evolution of the bosonic number operator $n = a^\dagger a$. Using Eq. (1), the corresponding Heisenberg equation for n can be derived when $[H,\rho] = 0$, yielding:

$$\langle n(t)\rangle = n_{\rm ss} + (\langle n(t=0)\rangle - n_{\rm ss})e^{-\gamma_c t}. \tag{2}$$

Since Eq. (1) applies to any motional mode undergoing cooling and heating, independently controlling these processes on several modes allows us to simultaneously realize engineered baths for multiple motional modes, each with an independently tunable temperature.

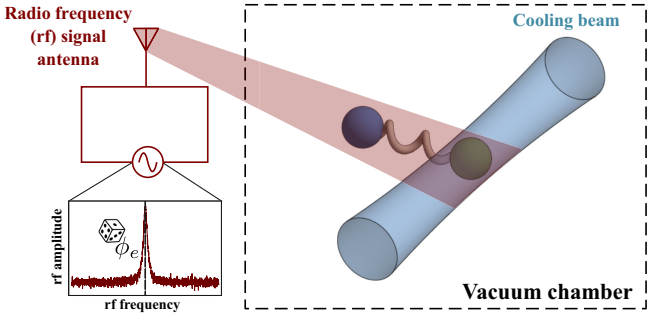


FIG. 1. Experimental setup for engineering a thermal reservoir with two trapped ions. Independent control of the bath temperature and dissipation rate is achieved by simultaneously applying motional cooling and heating to the relevant mode. Coolant ion is addressed with a cooling beam that removes phonon excitations from the collective vibrational mode (connecting spring between the two spheres). It is not necessary to apply cooling beams to all ions, as long as the addressed ion participates in the targeted motional mode. Concurrently, an antenna broadcasts electric-field signal with stochastic phases (ϕ_e) at the motional-mode frequency from outside the vacuum chamber that hosts the ions to induce motional heating. This setup can be straightforwardly extended to realize multimode thermal baths in longer ion chains.

Experimental setup—A finite-temperature bosonic reservoir can be engineered by applying laser-cooling beams in combination with electric-field signals that induce motional heating of a specific mode of the ion chain (see Fig. 1 and End Matter). By applying multiple frequency tones that address different motional modes, this setup enables the engineering of multimode reservoirs with individually controllable temperatures. Experimentally, tunable cooling rates for selected motional modes are achieved by applying multiple frequency components with different strengths to the laser-cooling beams, and injected electric-field signals with controlled-amplitude tones resonant with those modes and stochastically varying phases are used for heating. The experimental configurations used in this Letter are described in the End Matter.

Controlling thermal reservoirs—We demonstrate the control of thermal baths with independently tunable temperature and dissipation rate by simultaneously applying motional heating and cooling to a center-of-mass mode of a single trapped $^{171}Yb^+$ ion. The average phonon-number evolution of this motional mode is expected to follow Eq. (2), which we characterize experimentally as follows. We first prepare the motional mode to either $\langle n(t=0)\rangle \approx 7$ via Doppler cooling or $\langle n(t=0)\rangle \approx 0.1$ via resolved-sideband cooling, followed by a qubit-reset pulse to initialize the qubit in the $|\downarrow\rangle_z$ state. We then let the system evolve under the interaction with the engineered thermal bath described in Eq. (1) for time t. At the end of the evolution, we measure the phonon population $\langle n(t)\rangle$ by fitting the spin evolution under an anti-Jaynes-Cummings

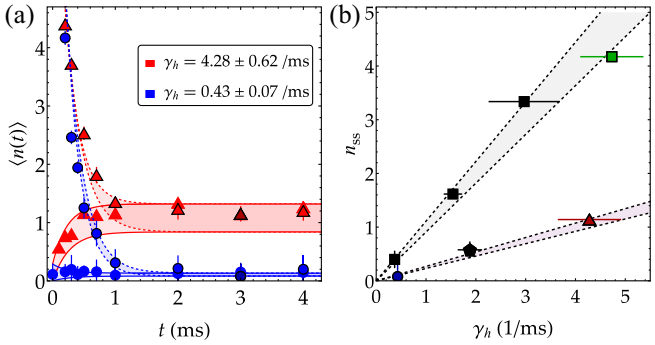


FIG. 2. Thermal bath controls. (a) Phonon-number dynamics from interacting with the engineered thermal bath. Red triangles and curves are associated with $\gamma_h = 4.28 \pm 0.62/\text{ms}$, while blue circles and curves correspond to $\gamma_h = 0.43 \pm 0.07/\text{ms}$. In both cases, $\gamma_c = 4.03 \pm 0.31/\text{ms}$. The curves are exponential functions with maximum and minimum time constants $1/\gamma_c$ and steady states given by $\langle n(t \to \infty) \rangle = \gamma_h/\gamma_c$. Data points with black outlines and dashed curves correspond to when the system starts from the Doppler-cooled temperature ($\langle n(t=0) \rangle \approx 7$), while data points with no outline and solid curves describe the realizations when the system is initialized from $\langle n(t=0) \rangle \approx 0.1$. Darkened data points are also used in (b) (and Fig. 5 of End Matter). (b) n_{ss} versus γ_h. Square data points correspond to the measured average phonon numbers after interacting with the engineered thermal bath, given by $\gamma_c = 1.00 \pm 0.10/\text{ms}$ and γ_h, for 6 ms, while data points of other shapes are associated with the measured average phonon numbers after interacting with the engineered thermal bath, given by $\gamma_c = 4.03 \pm 0.31/\text{ms}$ and γ_h, for 3 ms. The gray and purple bands are bounded by $\{\gamma_h/(\gamma_c = 1.00 - 0.10/\text{ms}), \gamma_h/(\gamma_c = 1.00 + 0.10/\text{ms})\}$ and $\{\gamma_h/(\gamma_c = 4.03 - 0.31/\text{ms}), \gamma_h/(\gamma_c = 4.03 + 0.31/\text{ms})\}$, respectively. Colored data points are used in Fig. 5 of End Matter.

Hamiltonian with the first-order blue-sideband drive (see End Matter). To measure the engineered γ_h and γ_c, we independently capture the $\langle n(t) \rangle$ evolutions under heating and cooling, respectively, following the same analysis used for their combined action in our thermal-bath engineering scheme. We then perform a linear fit to extract γ_h and an exponential fit to extract γ_c (see Supplemental Material [57] for calibrations). Knowing γ_h and γ_c allows us to predict $\bar{n} = n_{ss}$ and control it accordingly.

In Fig. 2(a), we show that the measured average phonon-number dynamics follow Eq. (2) for two engineered temperatures, starting from both a very low temperature [$\langle n(t=0) \rangle \approx 0.1$] and a Doppler-cooled temperature [$\langle n(t=0) \rangle \approx 7$]. We also observe that the average phonon numbers at long times (steady states) fall within the estimated range of $n_{ss} = \gamma_h/\gamma_c$ (indicated by the light red and blue bands for the higher- and lower-temperature cases, respectively). Moreover, we demonstrate control over the bath temperature, characterized by n_{ss}, from near zero (≈ 0.1, limited by the intrinsic heating rate of the motional mode) up to about 4 by varying the motional heating rate while independently controlling two different cooling rates [see Fig. 2(b)]. Our scheme is not limited to this temperature range, as increasing the heating rate or reducing the cooling rate could yield higher temperatures. We also show that the phonon-population probabilities in the steady states, fitted as free parameters, closely follow those of thermal states (see End Matter).

Finite-temperature charge transfer—The ability to independently control the bath temperature and dissipation rate enables a wide range of applications in quantum information science, particularly robust state preparation and engineered reservoirs for open-system quantum simulation. To showcase both capabilities, we investigate the nonequilibrium transfer dynamics of an electron between a donor electronic site ($|D\rangle \equiv |\uparrow\rangle_z$) and an acceptor electronic site ($|A\rangle \equiv |\downarrow\rangle_z$) that are collectively coupled to a damped vibrational mode held at a specific temperature.

This charge-transfer system can be described by a LVC Hamiltonian [40,63],

$$H = \frac{\Delta E}{2}\sigma_z + V\sigma_x + \frac{g}{2}\sigma_z(a^\dagger + a) + \omega a^\dagger a, \qquad (3)$$

where $\sigma_{x,z}$ are the Pauli operators, with ΔE and V denoting the donor-acceptor energy gap and coupling strength. The electronic sites are linearly coupled to a harmonic oscillator with vibrational energy ω, described by the creation ($a^\dagger$) and annihilation (a) operators, at a vibronic coupling strength g. Without electronic coupling, the vibronic system with $g \gtrsim \omega$ can be visualized as two displaced potential-energy surfaces with quantized energy levels: the donor surface is centered at $-g/2\omega$ and the acceptor surface at $+g/2\omega$ along the effective reaction coordinate, given by the position operator $y = y_0(a^\dagger + a)/2$, with $y_0 = \sqrt{1/2m\omega}$ and m being the particle mass [40,63].

When the electronic degree of freedom is strongly mixed ($V \sim g^2/4\omega$), the donor and acceptor energy surfaces hybridize into upper and lower adiabatic surfaces. This hybridization gives rise to eigenstates that are superpositions of donor and acceptor vibronic states, a hallmark feature of the strongly adiabatic regime of charge transfer. The absence of a perturbative parameter makes the transfer dynamics in this regime analytically challenging and therefore particularly interesting for experimental investigation.

Naturally, charge transfer occurs in condensed-phase environments [31], which can be modeled as a thermal reservoir. Under the conditions $\gamma \ll \omega$ and $\gamma \ll k_B T$, this reservoir can be described by Eq. (1) (with $\gamma \equiv \gamma_c$ and $\bar{n} \equiv n_{ss}$), where the bath temperature is given by $k_B T \approx \omega/\log(1 + 1/\bar{n})$ [40,63,64]. Under these conditions, the dissipation rate is also small compared with other relevant system parameters, such as g and V, while remaining nonnegligible on the relevant dynamical timescales. We also point out that the vibrational spectrum relevant to condensed-phase charge transfer, such as in Cytochrome

proteins [65], chlorophyll-based complexes [66], and bacteriochlorophyll-containing systems [67], includes low-frequency modes with ω spanning tens to a few hundred cm^{-1}, and higher-frequency intramolecular modes extending up to 1000 cm^{-1}. At room temperature ($T \simeq 300$ K), vibrational modes in the hundred cm^{-1} range correspond to thermal occupations $\bar{n} \simeq 0.01$–1, which is neither negligible nor large, making finite-temperature effects significant.

To jointly quantify the rate of dynamical equilibration and the amount of transferred population, we measure the inverse lifetime of the excitation residing in the donor site during the charge-transfer process [40,41,63,68], $k_T = [\int_0^{t_{\mathrm{sim}}} P_D(t)dt / \int_0^{t_{\mathrm{sim}}} tP_D(t)dt] - (2/t_{\mathrm{sim}})$, where t_{sim} is the simulation duration, and $P_D(t) = (\langle\sigma_z(t)\rangle + 1)/2$ [40,41,69] (see Supplemental Material [57] for details).

In Fig. 3(a), the blue curve and data points show that the low-temperature ($\bar{n} = 0.15$) transfer-rate spectrum in the strongly adiabatic regime ($V \sim g^2/4\omega$) exhibits two distinct behaviors with respect to the donor-acceptor energy gap (the experimental sequence is described in Supplemental Material [57]). At small energy offsets ($\Delta E < 2\omega$), the monotonically increasing region arises from strong electronic coupling to off-resonant hybridized states, while remaining limited by the dissipation rate. In this case, the transfer rates are approximately proportional to the dissipation rate [40,63]. When $\Delta E > 2\omega$, we experimentally observe resonant peaks at $\ell\omega$ for $\ell = 3$ and 4. Here, the initially localized donor state overlaps strongly with eigenstates of the upper-hybridized surface, which results in population trapping [40,41,63]. At these resonances, the trapped population is released during the dynamics, transferring from the upper- to the lower-hybridized surface. Simultaneously, dissipation in the presence of a low-temperature reservoir relaxes the wave packet into lower-energy levels of the lower-hybridized surface that strongly overlap with the acceptor site and are no longer resonant with the eigenenergy levels of the upper-hybridized surface, eventually driving the system to the steady state [see Fig. S6(B) in Supplemental Material [57]]. As ΔE increases, the transfer rates diminish due to the weak couplings between higher-energy hybridized states on the two surfaces, which are governed by the overlaps between their motional wave functions (namely, Franck-Condon factors), suppressing the transfer-rate resonances at $\Delta E \gtrsim 4\omega$.

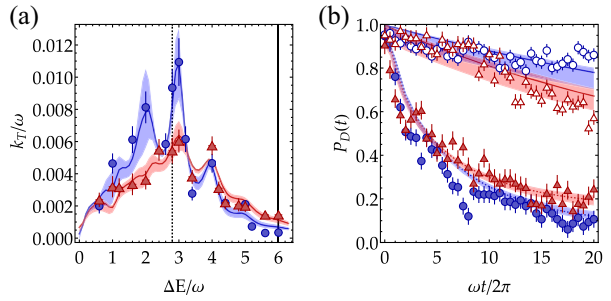


FIG. 3. Finite-temperature charge transfer. (a) Transfer rate versus donor-acceptor energy gap. Blue and red solid lines show the theoretical predictions of the transfer rate with $(V, g) = (0.2, 1.1)\omega$ in contact with thermal reservoirs characterized by $\bar{n} = 0.15$ and 0.80, respectively, at a dissipation rate of $\gamma = 0.036\omega$. These solid lines also consider experimental imperfections with $(\gamma_z, \gamma_m) = (0.0014, 0.0160)\omega$ (see Supplemental Material [57] for details). Blue-filled circles and red-filled triangles represent the corresponding experimental results with error bars obtained from resampling [40]. (b) Donor population dynamics. Blue curves and circles show theoretical and experimental results, respectively, for the system interacting with the $\bar{n} = 0.15$ reservoir, while red curves and triangles correspond to the $\bar{n} = 0.80$ reservoir. Dashed curves and filled data points are for $\Delta E = 2.8\omega$, and solid curves with open data points are for $\Delta E = 6.0\omega$. The shaded bands on the theoretical curves correspond to the mean uncertainty (± 0.20) in the most sensitive parameter in our setup, the bath temperature, and imperfect initial-state preparation.

When the bath temperature is increased to $\bar{n} = 0.80$ [red curve and data points in Fig. 3(a)], the transfer rates decrease at small donor-acceptor energy gaps but become slightly enhanced at larger gaps. This overall broadening of the spectrum can be attributed to the redistribution of thermal population across the hybridized energy surfaces: at higher temperatures, more population accumulates in higher-energy states. Consequently, for charge-transfer processes with small donor-acceptor gaps, higher temperatures place the initial donor population in higher-energy, hybridized states on both adiabatic surfaces, leaving a large fraction on the donor site [see Fig. S6(A) in Supplemental Material [57]] and thereby reducing transfer rates. This observation provides a new insight into the slope of the monotonically increasing region of the transfer-rate spectrum, which appears to be temperature-dependent in addition to its proportionality with the dissipation rate, found in Refs. [40,63]. On the other hand, when ΔE is sufficiently large ($\Delta E \gtrsim 4\omega$), thermal excitations redistribute the initially trapped donor population across eigenstates of the upper adiabatic surface, which are coherently transferred to the lower adiabatic surface at the $\Delta E = \ell\omega$ resonances, where ℓ is an integer [see Fig. S6(B) in Supplemental Material [57]]. For $g \gtrsim \omega$, the coupling rates for this process, determined by the Franck-Condon factors, increase at moderately high temperatures (see Supplemental Material [57] for details), leading to enhanced transfer rates. These effects have been predicted in more complex systems with long-range interactions [69]. We note that the details of the temperature effects depend on the system parameters (V, g, and ω).

Thermally activated transfer pathways in two-mode systems—We then simulate a LVC system featuring two dissipative vibrational modes ($\omega_1 > \omega_2$) in contact with thermal baths at different local temperatures and dissipation rates, described by [41]

$$H = V\sigma_x + \frac{\Delta E}{2}\sigma_z + \sum_{i=1}^{2}\left\{\frac{g_i}{2}\sigma_z\left(a_i + a_i^\dagger\right) + \omega_i a_i^\dagger a_i\right\}, \tag{4}$$

$$\frac{\partial\rho}{\partial t} = -i[H,\rho] + \sum_{i=1}^{2}\left\{\gamma_i(\bar{n}_i+1)\mathcal{L}_{a_i}[\rho] + \gamma_i\bar{n}_i\mathcal{L}_{a_i^\dagger}[\rho]\right\}. \tag{5}$$

In the vibrationally assisted exciton transfer regime ($g_i \ll \omega_i$), vibrational modes primarily act as mediators of exothermic transfer, enabling energy exchange at discrete resonances $\Delta E \approx \sqrt{(\ell_1\omega_1 + \ell_2\omega_2)^2 - (2V)^2}$, where ℓ_1 and ℓ_2 are integers [41,70]. For $0 < \Delta E < \omega_1$, only two resonances appear in the transfer-rate spectrum at very low temperature [blue curve and data in Fig. 4(a)], near $0.53\omega_1$ and $0.96\omega_1$, each corresponding to single-phonon exchange between the electronic system and one of the two vibrational modes. As shown by the red curve and data, raising the local temperature of the ω_2 mode selectively reduces the transfer rates associated with that mode's energy exchange, since stronger temperature-induced couplings adversely keep more population on the donor site during the dynamics (see Fig. S9 in Supplemental Material [57]). Interestingly, a mixed-mode resonance near $0.29\omega_1$ emerges, corresponding to excitation of the ω_1 mode and deexcitation of the ω_2 mode during coherent dynamics prior to equilibration. Despite the presence of dissipation, this transfer proceeds via interfering coherent pathways from combinations of phonon excitation and deexcitation. The blue curve and data also show that this process is suppressed when both modes are globally very cold (see Supplemental Material [57] for detailed explanations of these observations).

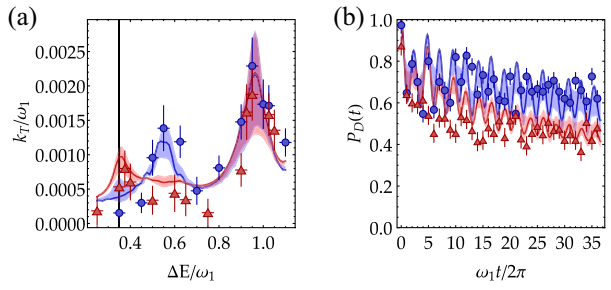


FIG. 4. Two-mode, vibrationally assisted exciton transfer at different local temperatures. (a) Transfer rate versus donor-acceptor energy gap. Blue and red solid lines show the theoretical predictions of the transfer rate with $(V, \omega_2, g_1, g_2) = (0.14, 0.60, 0.33, 0.18)\omega_1$ in contact with local thermal reservoirs characterized by $(\bar{n}_1, \bar{n}_2) = (0.10, 0.02)$ and (0.10,0.80), respectively, at dissipation rates $\gamma_1 = 0.013\omega_1$ and $\gamma_2 = 0.008\omega_2$. These solid lines also consider experimental imperfections with $(\gamma_z, \gamma_m) = (0.0004, 0.0040)\omega_1$ (see Supplemental Material [57] for details). Blue-filled circles and red-filled triangles represent the corresponding experimental results with error bars obtained from resampling [40]. (b) Donor population dynamics for $\Delta E = 0.35\omega_1$. Blue curves and circles show the theoretical and experimental results, respectively, for the system interacting with the $\bar{n}_2 = 0.02$ bath, while red curves and triangles correspond to the $\bar{n}_2 = 0.80$ bath. The shaded bands on the theoretical curves correspond to the mean uncertainty (± 0.20) in the most sensitive parameters in our setup, the bath temperatures, and imperfect initial-state preparation.

Outlook—In this Letter, we introduce a versatile and scalable method for engineering finite-temperature reservoirs for trapped-ion motion by balancing controlled heating induced by tailored broadcast electric-field signal with continuous resolved-sideband laser cooling. We experimentally demonstrate independent control over both bath temperatures and equilibration rates. Since high-temperature fits become increasingly sensitive to outlier populations and to drifts in motional mode frequencies or laser powers, we reconstruct thermal phonon distributions only up to $\bar{n} \lesssim 4$. However, this is an experimental, rather than fundamental, limitation, and the accessible temperature range could be extended through improved technical stability, refined analysis, and better heating and cooling protocols.

Applying this method to a dual-species trapped-ion setup, we realize charge-transfer dynamics across distinct thermal environments, gaining clearer insight into the role of temperature in the charge-transfer process in the strongly adiabatic regime. We observe that the temperature-induced distribution of excitation population across the mixed potential-energy landscape strongly shapes how the transfer-rate spectrum varies with the donor-acceptor energy gap. We also investigate local-temperature effects in two-mode, vibrationally assisted exciton transfer and find that local temperature can activate otherwise suppressed transfer pathways via constructive interference. These results confirm the role of temperature in LVC models and showcase our ability to tune the reservoir temperature in these open systems. This constitutes an important extension of previous trapped-ion LVC studies, which were restricted to either near-zero-temperature [40,41] or effectively infinite-temperature conditions [49,50].

Our method provides a useful tool for robust thermal-state preparation and for exploring finite-temperature open-system dynamics in purely bosonic and spin-boson models. With these capabilities, we move one step closer to emulating realistic chemical reactions [32,71], probing thermal entanglement [72,73], realizing high-efficiency quantum thermal machines [74,75], and examining quantum thermoelectric processes [76,77] to better understand the underlying mechanisms in their natural settings, as well as in the crossover conditions between the quantum and classical regimes [78]. Furthermore, resonantly driving higher-order motional processes with electric-field and laser-cooling tones offers a simple extension, opening avenues to nonlinear reservoirs and to structured, non-Gaussian bosonic equilibrium states. With this extension, one can explore dissipative quantum phase transitions and nonequilibrium dynamics with

nonlinear decays [79–81], as well as possibly stabilize nonclassical states that enhance protocols for bosonic computation and simulation [8,9]. Lastly, our technique not only expands the toolbox for trapped-ion quantum technologies but may also find applications in other bosonic platforms, particularly superconducting circuits.

Acknowledgments—G. P. acknowledges support from the Welch Foundation Award (Grant No. C-2154), the Office of Naval Research Young Investigator Program (Grant No. N00014-22-1-2282), the NSF CAREER Award (Grant No. PHY-2144910), and the Office of Naval Research (Grants No. N00014-23-1-2665 and No. N00014-24-1-2593). We acknowledge that this material is based on work supported by the U.S Department of Energy, Office of Science, Office of Nuclear Physics under the Early Career Award (Grant No. DE-SC0023806). The isotopes used in this research were supplied by the U.S. Department of Energy Isotope Program, managed by the Office of Isotope R&D and Production. H. P. acknowledges support from the NSF (Grant no. PHY-2513089) and the Welch Foundation (Grant No. C-1669).

Data availability—The data that support the findings of this article are publicly available [82].

[1] C. Monroe, W. C. Campbell, L.-M. Duan, Z.-X. Gong, A. V. Gorshkov, P. W. Hess, R. Islam, K. Kim, N. M. Linke, G. Pagano, P. Richerme, C. Senko, and N. Y. Yao, Programmable quantum simulations of spin systems with trapped ions, Rev. Mod. Phys. **93**, 025001 (2021).

[2] D. Wineland, C. Monroe, W. Itano, D. Leibfried, B. King, and D. Meekhof, Experimental issues in coherent quantum-state manipulation of trapped atomic ions, J. Res. Natl. Inst. Stand. Technol. **103**, 259 (1997).

[3] C. J. Myatt, B. E. King, Q. A. Turchette, C. A. Sackett, D. Kielpinski, W. M. Itano, C. Monroe, and D. J. Wineland, Decoherence of quantum superpositions through coupling to engineered reservoirs, Nature (London) **403**, 269 (2000).

[4] M. Brownnutt, M. Kumph, P. Rabl, and R. Blatt, Ion-trap measurements of electric-field noise near surfaces, Rev. Mod. Phys. **87**, 1419 (2015).

[5] W. Chen, J. Gan, J.-N. Zhang, D. Matuskevich, and K. Kim, Quantum computation and simulation with vibrational modes of trapped ions, Chin. Phys. B **30**, 060311 (2021).

[6] G. Pagano, W. Adamczyk, and V. So, Fundamentals of trapped ions and quantum simulation of chemical dynamics, arXiv:2505.20412.

[7] C. Flühmann, T. L. Nguyen, M. Marinelli, V. Negnevitsky, K. Mehta, and J. P. Home, Encoding a qubit in a trapped-ion mechanical oscillator, Nature (London) **566**, 513 (2019).

[8] V. G. Matsos, C. H. Valahu, T. Navickas, A. D. Rao, M. J. Millican, X. C. Kolesnikow, M. J. Biercuk, and T. R. Tan, Robust and deterministic preparation of bosonic logical states in a trapped ion, Phys. Rev. Lett. **133**, 050602 (2024).

[9] I. Rojkov, M. Simoni, E. Zapusek, F. Reiter, and J. Home, Stabilization of cat-state manifolds using nonlinear reservoir engineering, Phys. Rev. X **16**, 011056 (2026).

[10] D. Gottesman, A. Kitaev, and J. Preskill, Encoding a qubit in an oscillator, Phys. Rev. A **64**, 012310 (2001).

[11] M. H. Michael, M. Silveri, R. T. Brierley, V. V. Albert, J. Salmilehto, L. Jiang, and S. M. Girvin, New class of quantum error-correcting codes for a bosonic mode, Phys. Rev. X **6**, 031006 (2016).

[12] A. L. Grimsmo, J. Combes, and B. Q. Baragiola, Quantum computing with rotation-symmetric bosonic codes, Phys. Rev. X **10**, 011058 (2020).

[13] K. Toyoda, R. Hiji, A. Noguchi, and S. Urabe, Hong–ou–Mandel interference of two phonons in trapped ions, Nature (London) **527**, 74 (2015).

[14] S. Debnath, N. M. Linke, S.-T. Wang, C. Figgatt, K. A. Landsman, L.-M. Duan, and C. Monroe, Observation of hopping and blockade of bosons in a trapped ion spin chain, Phys. Rev. Lett. **120**, 073001 (2018).

[15] J. Zhang, M. Um, D. Lv, J.-N. Zhang, L.-M. Duan, and K. Kim, Noon states of nine quantized vibrations in two radial modes of a trapped ion, Phys. Rev. Lett. **121**, 160502 (2018).

[16] S. Ding, G. Maslennikov, R. Hablützel, and D. Matsukevich, Quantum simulation with a trilinear hamiltonian, Phys. Rev. Lett. **121**, 130502 (2018).

[17] O. Katz and C. Monroe, Programmable quantum simulations of bosonic systems with trapped ions, Phys. Rev. Lett. **131**, 033604 (2023).

[18] P.-Y. Hou, J. J. Wu, S. D. Erickson, D. C. Cole, G. Zarantonello, A. D. Brandt, S. Geller, A. Kwiatkowski, S. Glancy, E. Knill, A. C. Wilson, D. H. Slichter, and D. Leibfried, Coherent coupling and non-destructive measurement of trapped-ion mechanical oscillators, Nat. Phys. **20**, 1636 (2024).

[19] Z. Davoudi, N. M. Linke, and G. Pagano, Toward simulating quantum field theories with controlled phonon-ion dynamics: A hybrid analog-digital approach, Phys. Rev. Res. **3**, 043072 (2021).

[20] A. T. Than, S. V. Kadam, V. Vikramaditya, N. H. Nguyen, X. Liu, Z. Davoudi, A. M. Green, and N. M. Linke, Observation of quantum-field-theory dynamics on a spin-phonon quantum computer, arXiv:2509.11477.

[21] F. Zähringer, G. Kirchmair, R. Gerritsma, E. Solano, R. Blatt, and C. F. Roos, Realization of a quantum walk with one and two trapped ions, Phys. Rev. Lett. **104**, 100503 (2010).

[22] G. Clos, D. Porras, U. Warring, and T. Schaetz, Time-resolved observation of thermalization in an isolated quantum system, Phys. Rev. Lett. **117**, 170401 (2016).

[23] D. Lv, S. An, Z. Liu, J.-N. Zhang, J. S. Pedernales, L. Lamata, E. Solano, and K. Kim, Quantum simulation of the quantum rabi model in a trapped ion, Phys. Rev. X **8**, 021027 (2018).

[24] M.-L. Cai, Z.-D. Liu, W.-D. Zhao, Y.-K. Wu, Q. Mei, Y. Jiang, L. He, X. Zhang, Z.-C. Zhou, and L.-M. Duan, Observation of a quantum phase transition in the quantum Rabi model with a single trapped ion, Nat. Commun. **12**, 1126 (2021).

[25] Q.-X. Mei, B.-W. Li, Y.-K. Wu, M.-L. Cai, Y. Wang, L. Yao, Z.-C. Zhou, and L.-M. Duan, Experimental realization of

the Rabi-Hubbard model with trapped ions, Phys. Rev. Lett. **128**, 160504 (2022).
[26] S. Muralidharan and K. Toyoda, Site-dependent control of polaritons in the Jaynes–Cummings–Hubbard model with trapped ions, Appl. Phys. B **129**, 115 (2023).
[27] D. J. Gorman, B. Hemmerling, E. Megidish, S. A. Moeller, P. Schindler, M. Sarovar, and H. Haeffner, Engineering vibrationally assisted energy transfer in a trapped-ion quantum simulator, Phys. Rev. X **8**, 011038 (2018).
[28] C. H. Valahu, V. C. Olaya-Agudelo, R. J. MacDonell, T. Navickas, A. D. Rao, M. J. Millican, J. B. Pérez-Sánchez, J. Yuen-Zhou, M. J. Biercuk, C. Hempel, T. R. Tan, and I. Kassal, Direct observation of geometric-phase interference in dynamics around a conical intersection, Nat. Chem. **15**, 1503 (2023).
[29] J. Whitlow, Z. Jia, Y. Wang, C. Fang, J. Kim, and K. R. Brown, Quantum simulation of conical intersections using trapped ions, Nat. Chem. **15**, 1509 (2023).
[30] R. MacDonell, T. Navickas, T. Wohlers-Reichel, C. Valahu, A. Rao, M. Millican, M. Currington, M. Biercuk, T. Tan, C. Hempel, and I. Kassal, Predicting molecular vibronic spectra using time-domain analog quantum simulation, Chem. Sci. **14**, 9439 (2023).
[31] M. Kang, H. Nuomin, S. N. Chowdhury, J. L. Yuly, K. Sun, J. Whitlow, J. Valdiviezo, Z. Zhang, P. Zhang, D. N. Beratan, and K. R. Brown, Seeking a quantum advantage with trapped-ion quantum simulations of condensed-phase chemical dynamics, Nat. Rev. Chem. **8**, 340 (2024).
[32] V. C. Olaya-Agudelo, B. Stewart, C. H. Valahu, R. J. MacDonell, M. J. Millican, V. G. Matsos, F. Scuccimarra, T. R. Tan, and I. Kassal, Simulating open-system molecular dynamics on analog quantum computers, Phys. Rev. Res. **7**, 023215 (2025).
[33] K. J. Laidler, *Chemical Kinetics*, 3rd ed. (Harper & Row, New York, 1987).
[34] D. G. Truhlar, B. C. Garrett, and S. J. Klippenstein, Current status of transition-state theory, J. Phys. Chem. **100**, 12771 (1996).
[35] H.-P. Breuer and F. Petruccione, *The Theory of Open Quantum Systems* (Oxford University Press, New York, 2007).
[36] S. Fedortchenko, A. Keller, T. Coudreau, and P. Milman, Finite-temperature reservoir engineering and entanglement dynamics, Phys. Rev. A **90**, 042103 (2014).
[37] W. Wu and J.-B. Xu, Quantum coherence of spin-boson model at finite temperature, Ann. Phys. (Amsterdam) **377**, 48 (2017).
[38] G.-D. Lin and L.-M. Duan, Equilibration and temperature distribution in a driven ion chain, New J. Phys. **13**, 075015 (2011).
[39] J. F. Poyatos, J. I. Cirac, and P. Zoller, Quantum reservoir engineering with laser cooled trapped ions, Phys. Rev. Lett. **77**, 4728 (1996).
[40] V. So, M. Duraisamy Suganthi, A. Menon, M. Zhu, R. Zhuravel, H. Pu, P. G. Wolynes, J. N. Onuchic, and G. Pagano, Trapped-ion quantum simulation of electron transfer models with tunable dissipation, Sci. Adv. **10**, eads8011 (2024).
[41] V. So, M. Duraisamy Suganthi, M. Zhu, A. Menon, G. Tomaras, R. Zhuravel, H. Pu, P. G. Wolynes, J. N. Onuchic, and G. Pagano, Quantum simulation of charge and exciton transfer in multi-mode models using engineered reservoirs, Nat. Commun. **17**, 438 (2026).
[42] D. Kienzler, Quantum harmonic oscillator state synthesis by reservoir engineering, Ph.D. thesis, ETH Zürich, 2015, diss. ETH No. 22622.
[43] M. Cetina, L. N. Egan, C. Noel, M. Goldman, D. Biswas, A. R. Risinger, D. Zhu, and C. Monroe, Control of transverse motion for quantum gates on individually addressed atomic qubits, PRX Quantum **3**, 010334 (2022).
[44] C. Monroe, D. M. Meekhof, B. E. King, S. R. Jefferts, W. M. Itano, D. J. Wineland, and P. Gould, Resolved-sideband Raman cooling of a bound atom to the 3D zero-point energy, Phys. Rev. Lett. **75**, 4011 (1995).
[45] A. R. R. Carvalho, P. Milman, R. L. de Matos Filho, and L. Davidovich, Decoherence, pointer engineering, and quantum state protection, Phys. Rev. Lett. **86**, 4988 (2001).
[46] D. Kienzler, H.-Y. Lo, B. Keitch, L. de Clercq, F. Leupold, F. Lindenfelser, M. Marinelli, V. Negnevitsky, and J. P. Home, Quantum harmonic oscillator state synthesis by reservoir engineering, Science **347**, 53 (2015).
[47] M. Zhu, V. So, G. Pagano, and H. Pu, Dissipation-assisted steady-state entanglement engineering based on electron transfer models, Phys. Rev. A **112**, 012617 (2025).
[48] Y. Li, Y. Li, X. Cheng, L. Wang, X. Zhao, W. Hou, K. Rehan, M. Zhu, L. Yan, X. Qin, X. Peng, H. Yuan, Y. Lin, and J. Du, Programmable multi-mode entanglement via dissipative engineering in vibrating trapped ions, Sci. Adv. **11**, eadv7838 (2025).
[49] T. Navickas, R. J. MacDonell, C. H. Valahu, V. C. Olaya-Agudelo, F. Scuccimarra, M. J. Millican, V. G. Matsos, H. L. Nourse, A. D. Rao, M. J. Biercuk, C. Hempel, I. Kassal, and T. R. Tan, Experimental quantum simulation of chemical dynamics, J. Am. Chem. Soc. **147**, 23566 (2025).
[50] K. Sun, M. Kang, H. Nuomin, G. Schwartz, D. N. Beratan, K. R. Brown, and J. Kim, Quantum simulation of spin-boson models with structured bath, Nat. Commun. **16**, 4042 (2025).
[51] T. Behrle, T. L. Nguyen, F. Reiter, D. Baur, B. de Neeve, M. Stadler, M. Marinelli, F. Lancellotti, S. F. Yelin, and J. P. Home, Phonon laser in the quantum regime, Phys. Rev. Lett. **131**, 043605 (2023).
[52] Y. Li, Z. Xie, X. Yang, Y. Li, X. Zhao, X. Cheng, X. Peng, J. Li, E. Lutz, Y. Lin, and J. Du, Experimental realization and synchronization of a quantum van der pol oscillator, Sci. Adv. **11**, eady5649 (2025).
[53] J. M. Mayer, Proton-coupled electron transfer: A reaction chemist's view, Annu. Rev. Phys. Chem. **55**, 363 (2004).
[54] F. Fassioli, R. Dinshaw, P. C. Arpin, and G. D. Scholes, Photosynthetic light harvesting: Excitons and coherence, J. R. Soc. Interface **11**, 20130901 (2014).
[55] A. Jarmola, V. M. Acosta, K. Jensen, S. Chemerisov, and D. Budker, Temperature- and magnetic-field-dependent longitudinal spin relaxation in nitrogen-vacancy ensembles in diamond, Phys. Rev. Lett. **108**, 197601 (2012).
[56] H. J. Carmichael, *Statistical Methods in Quantum Optics 1: Master Equations and Fokker-Planck Equations* (Springer Science & Business Media, New York, 2013).
[57] See Supplemental Material at http://link.aps.org/supplemental/10.1103/mf8d-91ws for detailed derivations, additional

discussion, and supporting data, which includes Refs. [58–62].
[58] D. James, Quantum computation with hot and cold ions: An assessment of proposed schemes, Fortschr. Phys. **48**, 823 (2000).
[59] V. So, Trapped-ion quantum simulation of open-system chemical dynamics, Ph.D. thesis, Rice University, 2026.
[60] P.-Y. Hou, J. J. Wu, S. D. Erickson, G. Zarantonello, A. D. Brandt, D. C. Cole, A. C. Wilson, D. H. Slichter, and D. Leibfried, Indirect cooling of weakly coupled trapped-ion mechanical oscillators, Phys. Rev. X **14**, 021003 (2024).
[61] A. Chenu, M. Beau, J. Cao, and A. del Campo, Quantum simulation of generic many-body open system dynamics using classical noise, Phys. Rev. Lett. **118**, 140403 (2017).
[62] J. Johansson, P. Nation, and F. Nori, Qutip 2: A Python framework for the dynamics of open quantum systems, Comput. Phys. Commun. **184**, 1234 (2013).
[63] F. Schlawin, M. Gessner, A. Buchleitner, T. Schätz, and S. S. Skourtis, Continuously parametrized quantum simulation of molecular electron-transfer reactions, PRX Quantum **2**, 010314 (2021).
[64] A. Lemmer, C. Cormick, D. Tamascelli, T. Schaetz, S. F. Huelga, and M. B. Plenio, A trapped-ion simulator for spin-boson models with structured environments, New J. Phys. **20**, 073002 (2018).
[65] Y. Sun, A. Benabbas, W. Zeng, J. G. Kleingardner, K. L. Bren, and P. M. Champion, Investigations of heme distortion, low-frequency vibrational excitations, and electron transfer in cytochrome c, Proc. Natl. Acad. Sci. U.S.A. **111**, 6570 (2014).
[66] M. Rätsep, J. Linnanto, and A. Freiberg, Mirror symmetry and vibrational structure in optical spectra of chlorophyll a, J. Chem. Phys. **130**, 194501 (2009).
[67] C. Zhang, M. Gruebele, D. E. Logan, and P. G. Wolynes, Surface crossing and energy flow in many-dimensional quantum systems, Proc. Natl. Acad. Sci. U.S.A. **120**, e2221690120 (2023).
[68] S. S. Skourtis, A. J. R. Da Silva, W. Bialek, and J. N. Onuchic, New look at the primary charge separation in bacterial photosynthesis, J. Phys. Chem. **96**, 8034 (1992).
[69] D. Fallas Padilla, V. So, A. Menon, R. Zhuravel, H. Pu, and G. Pagano, Delocalized excitation transfer in open quantum systems with long-range interactions, PRX Quantum **6**, 040301 (2025).
[70] Z.-Z. Li, L. Ko, Z. Yang, M. Sarovar, and K. B. Whaley, Unraveling excitation energy transfer assisted by collective behaviors of vibrations, New J. Phys. **23**, 073012 (2021).
[71] R. A. Marcus, Electron transfer reactions in chemistry. Theory and experiment, Rev. Mod. Phys. **65**, 599 (1993).
[72] A. A. Valido, D. Alonso, and S. Kohler, Gaussian entanglement induced by an extended thermal environment, Phys. Rev. A **88**, 042303 (2013).
[73] T. Chanda, T. Das, D. Sadhukhan, A. K. Pal, A. Sen(De), and U. Sen, Emergence of entanglement with temperature and time in factorization-surface states, Phys. Rev. A **97**, 012316 (2018).
[74] J. Roßnagel, S. T. Dawkins, K. N. Tolazzi, O. Abah, E. Lutz, F. Schmidt-Kaler, and K. Singer, A single-atom heat engine, Science **352**, 325 (2016).
[75] G. Maslennikov, S. Ding, R. Hablützel, J. Gan, A. Roulet, S. Nimmrichter, J. Dai, V. Scarani, and D. Matsukevich, Quantum absorption refrigerator with trapped ions, Nat. Commun. **10**, 202 (2019).
[76] D. Roy and M. Di Ventra, Thermoelectric phenomena in disordered open quantum systems, Phys. Rev. B **81**, 193101 (2010).
[77] A. Tejero, R. Sánchez, L. E. Kaoutit, D. Manzano, and A. Lasanta, Asymmetries of thermal processes in open quantum systems, Phys. Rev. Res. **7**, 023020 (2025).
[78] P. F. Barbara, T. J. Meyer, and M. A. Ratner, Contemporary issues in electron transfer research, J. Phys. Chem. **100**, 13148 (1996).
[79] A. J. Shah, P. Kirton, S. Felicetti, and H. Alaeian, Dissipative phase transition in the two-photon Dicke model, arXiv:2412.14271.
[80] V. Y. Mylnikov, S. O. Potashin, G. S. Sokolovskii, and N. S. Averkiev, Emergent equilibrium and quantum criticality in a two-photon dissipative oscillator, Phys. Rev. Res. **7**, 013061 (2025).
[81] J. Liu, Q. Wu, J. E. Moore, H. Haeffner, and C. W. Wächtler, Observation of synchronization between two quantum van der pol oscillators in trapped ions, Phys. Rev. X **16**, 021062 (2026).
[82] V. So, Dataset for: Experimental realization of thermal reservoirs with tunable temperature in a trapped-ion spin-boson simulator, zenodo.21128021 10.5281/zenodo.21128021 (2026).

End Matter

Methods—In this Letter, we realize our proposed scheme by simultaneously performing continuous resolved-sideband cooling and inducing heating on a chosen motional mode. For the demonstration of thermal-bath control, we use the red-sideband drive via a 355 nm Raman transition together with a 370 nm optical pumping beam for cooling the motional mode of a single $^{171}Yb^{+}$ ion at the trap frequency of $\omega_c = 2\pi \times 3.904$ MHz (a center-of-mass radial mode) with an intrinsic heating rate of 0.43 ± 0.07/ms. The qubit used in this setup consists of the two hyperfine clock states of the $^{171}Yb^{+}$ electronic ground-state manifold: $|^2S_{1/2}, F = 1, m_F = 0\rangle \equiv |\uparrow\rangle_z$ and $|^2S_{1/2}, F = 0, m_F = 0\rangle \equiv |\downarrow\rangle_z$. For the application of this technique in quantum simulation of open systems, we drive the red-sideband process using quadrupole $|^2S_{1/2}\rangle \rightarrow |^2D_{3/2}\rangle$ transitions at 435.5 nm, along with a 935 nm repumper beam, on an ancilla $^{172}Yb^{+}$ ion cotrapped with the qubit $^{171}Yb^{+}$ ion. This results in sympathetic cooling of the shared motional mode at $\omega_t = 2\pi \times 3.776$ MHz (an out-of-phase radial mode) with an intrinsic heating rate of 0.03 ± 0.01/ms, corresponding to the axial trap frequency of $\omega_a \approx 2\pi \times 0.99$ MHz. The qubit ion is simultaneously addressed by 355 nm Raman beams to engineer the LVC

Hamiltonians [40,41] (see Supplemental Material [57] for details). Together with motional heating, this enables us to investigate the effects of temperature on the out-of-equilibrium dynamics of excitation transfer models.

Motional heating is induced by driving the ion chain with a radio frequency (rf) electric field at the selected motional-mode frequency. The rf signal is delivered via an antenna mounted near the vacuum system (Fig. 1, see Supplemental Material [57] for details), and its phase is varied stochastically. The drive therefore produces coherent displacements of the addressed motional mode whose direction in motional phase space varies randomly in time, resulting in a random-walk trajectory. When averaged over many uncorrelated trajectories, this random walk yields phase-space diffusion that can be approximated as Markovian heating within a Lindblad master-equation framework [50,59]. In practice, we implement this by applying the drive in many small time steps with independently randomized phases within each realization, and then averaging the resulting dynamics over many realizations. For the Lindblad approximation to be valid, the time step must be short compared to all other relevant dynamical timescales in the system [50]. In Fig. 2, each data point is given by 40 random phase sequences, where each sequence consists of multiple phase-varying steps with a fixed time step of 0.05 ms and is repeated 30 times. We note that for large n_{ss}, more sequences are required to obtain a well-approximated thermal distribution of the phonon population, as discussed in Ref. [50]. For $n_{ss} \approx 4$, we use 60 sequences.

We also find that, in the presence of motional dephasing, a stochastic-phase drive applied without temporal discretization can produce dynamics and steady states that are experimentally comparable to those predicted by the Lindblad thermal-bath master equation for relatively low temperature baths ($\bar{n} \lesssim 1$) when combined with cooling and averaged over many realizations (see Supplemental Material [57] for details). This approach enables higher data-taking rates and reduces calibration complexity, and we use it in the LVC-model simulations (Figs. 3 and 4).

Moreover, we note that motional heating can also be achieved either by directly injecting broadband noise into an ion-trap electrode [3,49] or by combining red- and blue-sideband optical drives with stochastic phases [32,50]. A theoretical exploration of combining the latter method with qubit reset operations as an alternative approach for finite-temperature bath engineering is provided in Supplemental Material [57]. Realizing a Markovian bath with broadband noise requires a correlation time much shorter than the relevant system timescales (i.e., a bandwidth much larger than the system's characteristic frequencies), which can reduce mode selectivity by simultaneously driving multiple

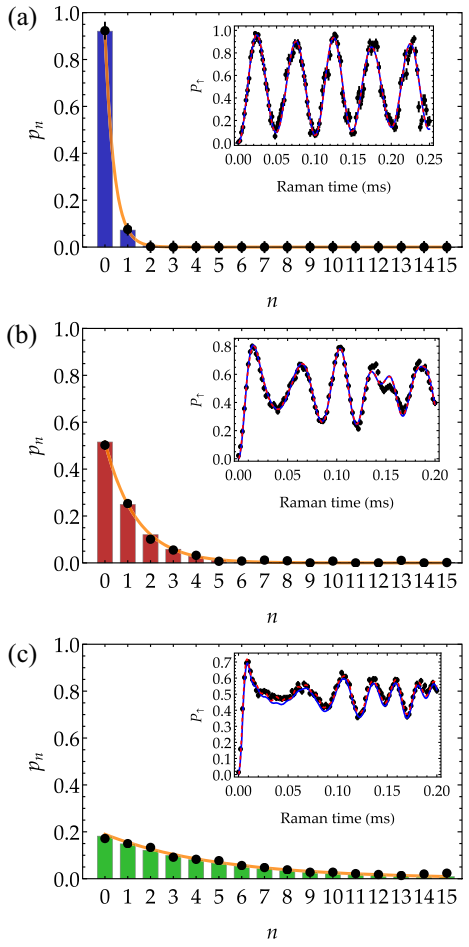


FIG. 5. Steady-state phonon-number distribution from the engineered thermal reservoir. (a) $\gamma_c = 4.03 \pm 0.31/\text{ms}$ and $\gamma_h = 0.43 \pm 0.07/\text{ms}$ for 3 ms (dark blue in Fig. 2 of the main text), (b) $\gamma_c = 4.03 \pm 0.31/\text{ms}$ and $\gamma_h = 4.28 \pm 0.62/\text{ms}$ for 3 ms (dark red in Fig. 2 of the main text), and (c) $\gamma_c = 1.00 \pm 0.10/\text{ms}$ and $\gamma_h = 4.73 \pm 0.62/\text{ms}$ for 6 ms [green in Fig. 2(b) of the main text]. Each inset corresponds to the spin dynamics of the steady-state system undergoing the probe blue-sideband drive for the phonon-number distribution measurement (black data points in the main figure). Bar charts represent the best-fitted thermal state bounded by γ_h/γ_c: (a) 0.09 ± 0.02, (b) 0.94 ± 0.05, and (c) 4.50 ± 0.19. The orange solid curves denote the corresponding fits to the thermal-state distribution functions, with reduced chi-square values (χ^2_{red}) of 0.005, 0.43, and 0.91, respectively. The low reduced chi-square value in (a) suggests that the assigned error bars are likely overestimated, as they were inferred from shot-noise-limited data taken with only 150 experimental repetitions in the absence of engineered heating. In contrast, the error bars and fits are reasonable for (b) and (c), which were obtained using 1200 and 1800 repetitions, respectively, where larger sample sizes were required to approximate Markovian motional heating. Dashed red and solid blue curves in the insets describe the dynamics of the fitted phonon-number distribution and the estimated thermal state, respectively.

modes in mode-crowded chains. Therefore, this approach is better suited to global-heating protocols, where mode selectivity is not required. On the other hand, a stochastically varying-phase drive can preferentially heat a chosen mode, provided that the displacement drive's Rabi coupling strength and detuning are smaller than the mode spacing. This makes the latter approach a scalable route to mode-selective heating.

To extract the phonon-number distribution of the motional state, we apply an anti-Jaynes-Cummings Hamiltonian using the first-order blue-sideband drive and fit the measured spin dynamics to

$$P_{\uparrow}(t, t_{\mathrm{p}}) = \frac{1}{2}\sum_{n} p_n(t)[1 - e^{-\gamma_{\mathrm{d}} t_{\mathrm{p}}} \cos(\Omega t_{\mathrm{p}}\sqrt{n+1})], \quad \text{(A1)}$$

where $p_n(t)$ is the population in Fock state $|n\rangle$ at the evolution time t, γ_{d} is an empirical decay constant given by spin and motional decoherences in the system, t_{p} is the duration of the blue-sideband drive, and Ω corresponds to the sideband Rabi frequency. From the fitted $p_n(t)$, we can calculate the average phonon excitation of the motional mode $\langle n(t)\rangle$, whose standard deviation is obtained from the covariance matrix of the fitting results [24]. For the fits, we apply loose constraints to suppress extreme outliers that could distort the evaluation of $\langle n(t)\rangle$ (see Supplemental Material [57] for details).

Steady-state phonon-number distributions—We show in Fig. 5 that the phonon-population distributions of the steady states in Fig. 2 of the main text resemble those of thermal states. We compare the free-fit estimates (black points) with the thermal distributions (colored bars), whose best-fit average phonon numbers are constrained by the measured values of γ_h/γ_c and their uncertainties. While the present measurements do not directly reconstruct the off-diagonal elements of the density matrix, motional coherences in the Fock basis are not expected for the engineered reservoirs studied here. The applied electric-field modulation is effectively incoherent and randomized, while continuous resolved-sideband cooling provides both energy and coherence relaxation. Together, these processes suppress phase coherence in the motional Fock basis. In addition, the measured Fock-state populations agree well with fitted thermal-state distributions, and motional Ramsey spectroscopy between $|0\rangle$ and $|1\rangle$ of the center-of-mass mode gives a typical upper-bound motional coherence time of 1.3 ms in our setup. These observations support the interpretation that the prepared motional states are thermal within our experimental resolution.